OXFORD

Cerebral Cortex, 2024, **34**, 1–10
https://doi.org/10.1093/cercor/bhad491
Advance access publication date 18 December 2023
Original Article

Cortical myelin and thickness mapping provide insights into whole-brain tumor burden in diffuse midline glioma

Simin Zhang[1,2], Xibiao Yang[3,4], Qiaoyue Tan[5], Huaiqiang Sun[1,2], Di Chen[1,2], Yinying Chen[4], Hongjing Zhang[6,7], Yuan Yang[8], Qiyong Gong[1,9,*], Qiang Yue[4,6,*]

[1]Huaxi MR Research Center (HMRRC), Department of Radiology, West China Hospital of Sichuan University, Chengdu 610041, China,
[2]Research Unit of Psychoradiology, Chinese Academy of Medical Sciences, Chengdu 610072, China,
[3]Functional and Molecular Imaging Key Laboratory of Sichuan Province, West China Hospital of Sichuan University, Chengdu 610041, China,
[4]Department of Radiology, West China Hospital of Sichuan University, Chengdu 610041, China,
[5]Division of Radiation Physics, State Key Laboratory of Biotherapy and Cancer Center, West China Hospital of Sichuan University, Chengdu 610041, China,
[6]Huaxi Glioma Center, West China Hospital of Sichuan University, Chengdu 610041, China,
[7]Department of Radiology, West China School of Public Health and West China Fourth Hospital, Sichuan University, Chengdu 610065, China,
[8]Department of Neurosurgery, West China Hospital of Sichuan University, Chengdu 610041, China,
[9]Department of Radiology, West China Xiamen Hospital of Sichuan University, Xiamen 610041, China

*Corresponding authors: Dr. Qiyong Gong, Department of Radiology, West China Xiamen Hospital of Sichuan University, 699 Jinyuan Xi Road, Jimei District, 361021 Xiamen, Fujian, China. Email: qiyonggong@hmrrc.org.cn; Prof. Qiang Yue, Department of Radiology, West China Hospital of Sichuan University, #37 GuoXue Xiang, Chengdu, Sichuan 610041, China. Email: scu_yq@163.com

Systemic infiltration is a hallmark of diffuse midline glioma pathogenesis, which can trigger distant disturbances in cortical structure. However, the existence and effects of these changes have been underexamined. This study aimed to investigate whole-brain cortical myelin and thickness alternations induced by diffuse midline glioma. High-resolution T1- and T2-weighted images were acquired from 90 patients with diffuse midline glioma with H3 K27-altered and 64 patients with wild-type and 86 healthy controls. Cortical thickness and myelin content was calculated using Human Connectome Project pipeline. Significant differences in cortical thickness and myelin content were detected among groups. Short-term survival prediction model was constructed using automated machine learning. Compared with healthy controls, diffuse midline glioma with H3 K27-altered patients showed significantly reduced cortical myelin in bilateral precentral gyrus, postcentral gyrus, insular, parahippocampal gyrus, fusiform gyrus, and cingulate gyrus, whereas diffuse midline glioma with H3 K27 wild-type patients exhibited well-preserved myelin content. Furtherly, when comparing diffuse midline glioma with H3 K27-altered and diffuse midline glioma with H3 K27 wild-type, the decreased cortical thickness in parietal and occipital regions along with demyelination in medial orbitofrontal cortex was observed in diffuse midline glioma with H3 K27-altered. Notably, a combination of cortical features and tumor radiomics allowed short-term survival prediction with accuracy 0.80 and AUC 0.84. These findings may aid clinicians in tailoring therapeutic approaches based on cortical characteristics, potentially enhancing the efficacy of current and future treatment modalities.

Key words: cortical myelin content; cortical thickness; diffuse midline glioma; H3 K27-altered; whole-brain tumor burden.

Introduction

Diffuse midline glioma (DMG) represents a subset of brain tumors primarily impacting the pediatric and adolescent populations (Chintagumpala et al. 2015; Louis et al. 2016). Patients diagnosed with DMG typically exhibit an overall survival of 9–11 months, with less than 10% of them surviving beyond the two-year mark post-diagnosis. The high mortality rate makes DMG the leading cause of death in children with central nervous system tumors (Hoffman et al. 2018). Notably, Global hypomethylation of histone H3 K27 is frequently observed in cases of DMG. This phenomenon arises from recurring somatic mutations in H3 genes or through overexpression of the Enhancer of Zest Homologs Inhibitory Protein in patients (Louis et al. 2016; Sievers et al. 2021). Consequently, based on these genetic alternations, DMG has been categorized into two distinct subtypes: H3 K27-altered (DMG-A) and wild-type (DMG-W; Louis et al. 2021).

Due to the rarity of the disease and the high risks of surgical resections and biopsies, DMG is still poorly characterized. The challenges inherent in our current therapeutic approaches indicate that the underlying mechanism of DMG progression is not sufficiently elucidated (Noon and Galban 2023). Recent studies have demonstrated that glioma is a systematic disease wherein tumor cells spread far beyond the macroscopically visible lesion and form a functional network throughout the entire brain (Sahm et al. 2012; Osswald et al. 2015). Thus, assessing the whole brain tumor burden in DMG could offer vital insights into the progression of the tumor in the individual patient. This, in turn, would enable risk stratification and allow for personalized treatment strategies.

Received: October 30, 2023. **Revised:** November 21, 2023. **Accepted:** November 22, 2023

Invasive growth along the white matter (WM) tract is recognized as an important clinicopathologic characteristic of gliomas (Giese and Westphal 1996; Wang et al. 2019; Duffau 2022). Prior studies have shown widespread damage and demyelination of long-range axons in the normal-appearing WM in patients with DMG (Thust et al. 2020; Zhang et al. 2022). Notably, myelinated axons are most prominent in the brain's deep WM, they are also abundant within the cerebral cortex gray matter, where both the initial and terminal processes of large pyramidal cells, as well as the short-range axonal processes of cortical interneurons, frequently exhibit heavy myelination (Nieuwenhuys 2013). DMG, which preferentially migrate along the surface of demyelinated axons be may also induced abnormalities in cortical myelin and thickness (Wang et al. 2019). These changes could potentially serve as biomarkers for a more comprehensive assessment of the whole-brain tumor burden in DMG, while simultaneously complementing measurements of myelination outside the deep WM structures.

Nevertheless, non-invasively and feasibly mapping cortical myelin during routine scans remains a formidable challenge. A novel technique based on the ratio between T1- and T2-weighted (T1w/T2w) structural imaging intensities has emerged as a promising tool for estimating cortical myelin content in vivo (Glasser et al. 2016; Mendez Colmenares et al. 2021). The myelin mapping derived from the T1w/T2w ratio has been demonstrated to converge with histological maps of cortical myelin (Nieuwenhuys and Broere 2017). Also, the T1w/T2w ratio has been applied in clinical studies in order to identify brain regions showing associations of their myelin content with neurological disorders including Alzheimer's disease (Fernandez-Alvarez et al. 2022), Huntington's disease (Rowley et al. 2018), multiple sclerosis (Righart et al. 2017). Recent studies found that the T1w/T2w ratio has overall high reproducibility and has advantages over R1 when conducting cortical segmentation (Nerland et al. 2021). Collectively, the aforementioned research indicates that the myelin mapping technique offers pertinent insights into brain organization and cortical function, and is sensitive to disease states. However, this approach has not previously been explored in DMG- related damage.

In the present study, we aimed to investigate whole-brain tumor burden induced by DMG based on cortical myelin and thickness mapping, and identify a non-invasive cortical biomarker to differentiate H3 K27 altered subtype from DMG, furtherly, we intended to assess the potential value of cortical features in short-term survival prediction in DMG. We hypothesized that there would be altered cortical myelin and thickness in patients with DMG compared with healthy controls (HC). Given that prior research supports glioma-induced microstructural reorganizations are intricately linked to the underlying genotype status (Price et al. 2016). Therefore, we also hypothesized that DMG patients harboring H3 K27 altered would exhibit specific cortical myelin and thickness reorganization patterns. Moreover, we also hypothesized that cortical metrics would help classifying patients with short-term survival from DMG at the individual level with significant accuracy.

Materials and methods

Participants

This study received approval from the ethics committee at West China Hospital of Sichuan University, and written informed consent was obtained from all participants. The main inclusion criteria were as follows: (i) patients have a pathological diagnosis of DMG and confirmation of H3K27 mutant status via gene sequencing; (ii) all patients underwent preoperative three-dimensional T1-weighted images (3DT1WI) and three-dimensional T2-weighted images (3DT2WI); (iii) to ensure homogeneity of tumor location, only DMG involved infratentorial midline structures including brainstem (midbrain, pontine, and medulla oblongata), fourth ventricle, peri-fourth ventricle and cerebellum were selected; and (iv) without relevant treatment history before the MR scanning. The primary endpoint was overall survival (OS), which was defined as the number of days from the initial pathological diagnosis to death (censored = 1) or the last date that they were known to be alive (censored = 0). Finally, a total of 90 patients with DMG, DMG-A and 64 patients with DMG-W were consecutively enrolled in this study. Furthermore, 86 healthy participants matched for age, sex, and education level were recruited as HC. The participants' enrollment process is shown in Fig. S1.

MRI scanning protocols

Data were collected on a Siemens 3 T Trio MRI scanner using a 12-channel head coil. The protocol was as follows: (i) 3DT1WI were acquired by a magnetization-prepared rapid gradient-echo sequence: Repetition time (TR) = 1550 ms, echo time (TE) = 2 ms, Inversion time (TI) = 900 ms, flip angle = 9°, matrix size = 256 × 232, field of view (FOV) = 230 × 254 mm^2, slice thickness = 1 mm. (ii) 3DT2WI were acquired by a 3D turbo spin-echo sequence with variable flip-angle echo trains (SPACE): TR = 2000 ms, TE = 350 ms, flip angle = 120°. The geometric parameters are same with 3DT1WI scan protocol. (iii) fluid-attenuated inversion recovery (FLAIR): TR = 6000 ms; TE = 81 ms; TI = 2028.3 ms; flip angle = 150°; matrix size = 320 × 196; FOV = 192 × 220 mm^2; slice thickness = 5 mm; and (iv) gadolinium-enhanced (Multihance, Braccosine, Shanghai, China) 3D T1-weighted images (Gd-3DT1WI) were acquired using the same scanning parameters as 3DT1WI.

DMG segmentation

We employed 3D U-net for automatically segment DMG, a deep learning approach that has shown its reliability and efficiency in previous study (Isensee et al. 2021). Subsequently, a mask encompassing the entire tumor region was generated, segmentation results were shown in Fig. S2. Each mask underwent visual evaluation by two neuroradiologists independently, who utilized ITK-SNAP 3.6.0 software (Z.H.J and Y.X.B, both possessing over a decade of experience in neuro-oncology). For each patient, a comprehensive set of 558 radiomics features was extracted using the "PyRadiomics" package, which is implemented in Python. Further details regarding the segmentation procedures and the extraction of radiomics features can be found in the Supplementary Information section.

Structural MRI data preprocessing

The cortical surfaces were created using the structural Human Connectome Project (HCP) pipeline (Glasser and Van Essen 2011). The pipeline is comprised of three sections: preFreeSurfer, FreeSurfer, and postFreeSurfer. The preFreeSurfer section was performed to bring the T1w and T2w images into alignment and to correct imaging distortion to minimize the artifacts. In the FreeSurfer section, cortical surfaces were generated from each orientation normalized T1w/T2w pair using FreeSurfer recon-all processing pipeline. This step included brain extraction, automated tissue segmentation, generation of WM and pial

surfaces, surface topology correction, inflation of surfaces, and spherical registration. Following the FreeSurfer section, cortical myelin maps were generated for further analysis and presentation. A mid-thickness surface was created for each subject by averaging the white and pial surfaces. Afterwards, the mid-thickness surfaces were registered across subjects to create a group surface, which was resampled to a resolution of 164 k vertices and then down-resampled to a low-resolution of 32 k vertices for statistical analysis.

Cortical myelin and thickness mapping

Each image underwent a thorough inspection, and any segmentation errors were manually corrected by a trained investigator who was blinded to the subjects' identities (Fig. S3). The T1w/T2w ratio within cortical ribbon were mapped to individual's native mid-thickness surface. Afterwards, T1w/T2w images were deformed and resampled from the native mid-thickness surface to the 32 k fsaverage surface. The ratio images were smoothed along the 32 k fsaverage surface using a Gaussian smoothing kernel ($\sigma = 2$). These T1w/T2w ratio maps represent cortical myelin content at each vertex on the cortical surface (Glasser and Van Essen 2011).

Cortical thickness was obtained by calculating the shortest distance from the gray/white boundary to the gray/cerebrospinal fluid boundary at each vertex of the tessellated surface (Fischl 2012).

Statistical analysis

The normality of continuous variables was assessed using the Shapiro–Wilk test. For normally distributed data, either a one-way analysis of variance (ANOVA) or t-test was employed, while the Kruskal–Wallis test was utilized for non-normally distributed data. In this study, all continuous variables exhibited normal distribution. Consequently, group differences (DMG-A, DMG-W, and HC) were assessed with ANOVA (age and educational level) and χ^2 test (sex). Patients' group difference in Karnofsky Performance Status (KPS) score were compared using a two-sample *t*-test. The significance value was set at $P < 0.05$.

A general linear model was applied to assess group differences in myelin content and cortical thickness at the level of each vertex for each hemisphere separately, when an F-test is significant, individual t-tests are used to determine the direction of the effect. During the calculations, we set gender, age, and educational level as covariates. Statistical test was performed using permutation test implemented in FSL/PALM package (https://fsl.fmrib.ox.ac.uk/fsl/fslwiki/PALM) (Winkler et al. 2014). For each contrast, significant clusters were determined using 5000 permutations with the threshold-free cluster enhancement method combined with family-wise error correction at $P < 0.05$ for multiple comparisons. The anatomical locations of significant clusters were determined based on the Desikan–Killiany atlas.

When a significant group difference was identified, we extracted the value of mean cortical myelin content and thickness in the significant cluster for each subject. Pearson's correlation coefficients (r) were calculated to assess the relationship between cortical alterations and DMG's radiomics features. A *P*-value < 0.05 was considered statistically significant for correlation analyses.

The short-term survival classification models were created by automatic machine learning (ML) framework, named Pycaret, which is a Python wrapper for a number of ML algorithms and packages. The target response for each model was the patient's OS grouped into two classes to distinguish patients who survived < 12 months (short-term survivors) from others. Details of Pycaret analysis are described in supplementary materials (Fig. S4). The image processing and statistical analysis workflow are shown in Fig. 1.

Results

Participant characteristics

Based on our inclusion criteria, 90 patients with DMG-A (mean age, 13.51 years; range, 6–47 years, sex ratio, 52 male/38 female), 64 patients with DMG-W (mean age, 16.17 years; range, 7–56 years; sex ratio, 38 male/26 female), and 86 HC (mean age, 14.57 years; range, 7–52 years; sex ratio, 55 male/31 female) were recruited in this study. There were no significant differences in age ($P = 0.129$), sex ($P = 0.690$), or years of education ($P = 0.154$) among above three groups. KPS score also showed no significant differences between patients' group ($P = 0.240$). Table 1 presents group demographic and clinical background variables.

Diffuse midline glioma with H3 K27-altered vs. healthy controls

Compared with HC, DMG-A group had significantly lower cortical myelin content in the cluster involving the bilateral precentral gyrus (PreCG), postcentral gyrus (PoCG), insular, isthmus cingulate gyrus (ICG), parahippocampal gyrus (PHG), fusiform gyrus (FG), right posterior cingulate gyrus (PCG), caudal anterior cingulate gyrus (cACG) (Fig. 2A). Regarding cortical thickness, patients with DMG-A exhibited widespread cortical thickening predominantly in frontal, parietal and occipital lobes compared with HC (Fig. 2B).

Diffuse midline glioma with H3 K27 wild-type vs. healthy controls

There was no significant brain cluster was found in cortical myelin content between the DMG-W group and HC. However, the DMG-W group exhibited greater cortical thickness in the bilateral frontal and occipital lobes (Fig. 2C).

Diffuse midline glioma with H3 K27-altered vs. diffuse midline glioma with H3 K27 wild-type

Compared with the DMG-W, the DMG-A group showed significantly lower cortical myelin content in the bilateral paracentral gyrus (PaCG), preCG, insular, PCG, cACG and medial orbitofrontal gyrus (MOFG) (Fig. 3A). With respect to cortical thickness, DMG-A patients showed decreased cortical thickness in bilateral parietal and occipital lobes compared with the DMG-W patients (Fig. 3B).

The relationship between cortical structure and DMG radiomics features

No significant correlations were found between altered cortical myelin or thickness in DMG-W group and radiomics features. However, the DMG-A group radiomics features including Gray Level Run Length Matrix of Gray Level Non-Uniformity (GLRLM_GLN) ($P = 0.00012$, $r = 0.631$) and Shape of Major Axis Length (Shape_MAL) ($P = 0.00015$, $r = 0.540$) showed significant positive correlation with cortical thickness in the regions of bilateral frontal, parietal, and occipital lobes (Fig. 4).

Short-term survival prediction models created by Pycaret

For the models fitted to tumor radiomics data, the catboost classifier performed best, with accuracy 0.72 and AUC 0.78 (Fig. 5A), while after incorporating whole-brain cortical myelin and thickness into the radiomics model, the AUC of best

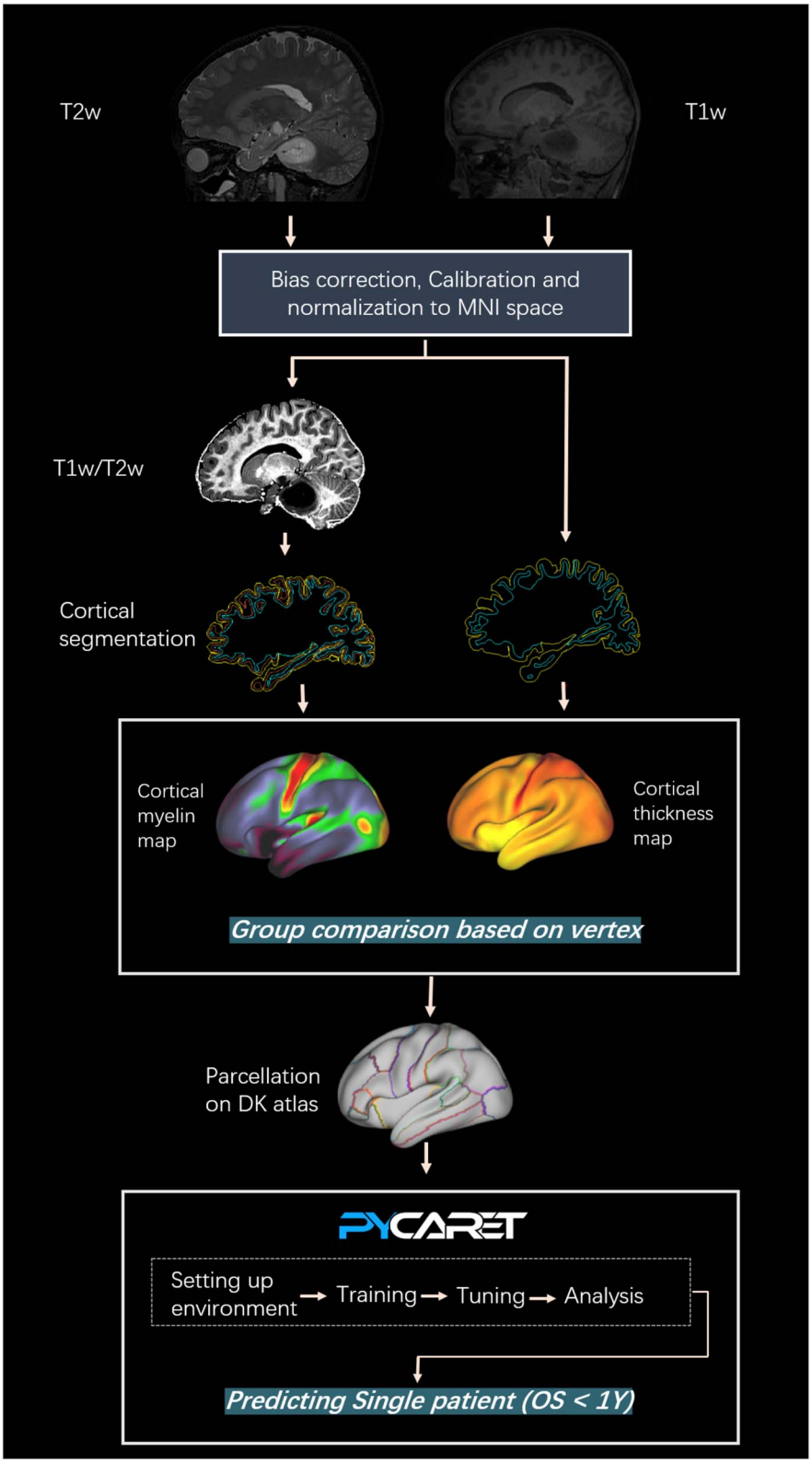

Fig. 1. Study workflow. First, high-resolution T1w and T2w structural images of participants were preprocessed and generated the T1w/T2w images based on HCP pipeline. Next, cortical myelin content was obtained by computing the ratio of T1w to T2w at each vertex, while cortical thickness was determined by measuring the shortest distance from the gray/white boundary to the gray/cerebrospinal fluid boundary at each vertex. Group differences were detected among DMG-A, DMG-W, and HC at each vertex. Further, cortical myelin content and thickness values were extracted based on DK atlas and these cortical metrics were subsequent fed into Pycaret framework (an automated machine learning tool) for construction of predictive models aimed at identifying DMG patients with short-term survival. Abbreviations: DMG-A, diffuse midline glioma with H3 K27-altered; DMG-W, diffuse midline glioma with H3 K27 wild-type; HC, healthy controls; DK atlas, Desikan–Killiany atlas.

Table 1. General characteristics of the participants.

	DMG-A	DMG-W	HC	P-values
No.	90	64	86	NA
Age (mean, range), years	13.51 ± 6.84 (6–47)	16.17 ± 9.78 (7–56)	14.57 ± 8.71(7–52)	0.129
Sex ratio, M/F, *n*	52/38	38/26	55/31	0.690
Education, years	5.69 ± 4.89	6.64 ± 4.38	6.70 ± 5.02	0.154
KPS	72.11 ± 8.21	79.77 ± 9.14		0.240
Tumor location				
Brainstem	67	41		
Fourth ventricle or peri-fourth ventricle	9	4		
Cerebellum	14	19		

Abbreviations: DMG-A = diffuse midline glioma, H3 K27-altered; DMG-W = diffuse midline glioma, H3 K27 wild-type; HC = healthy control; NA = not applicable; KPS = Karnofsky Performance Status.

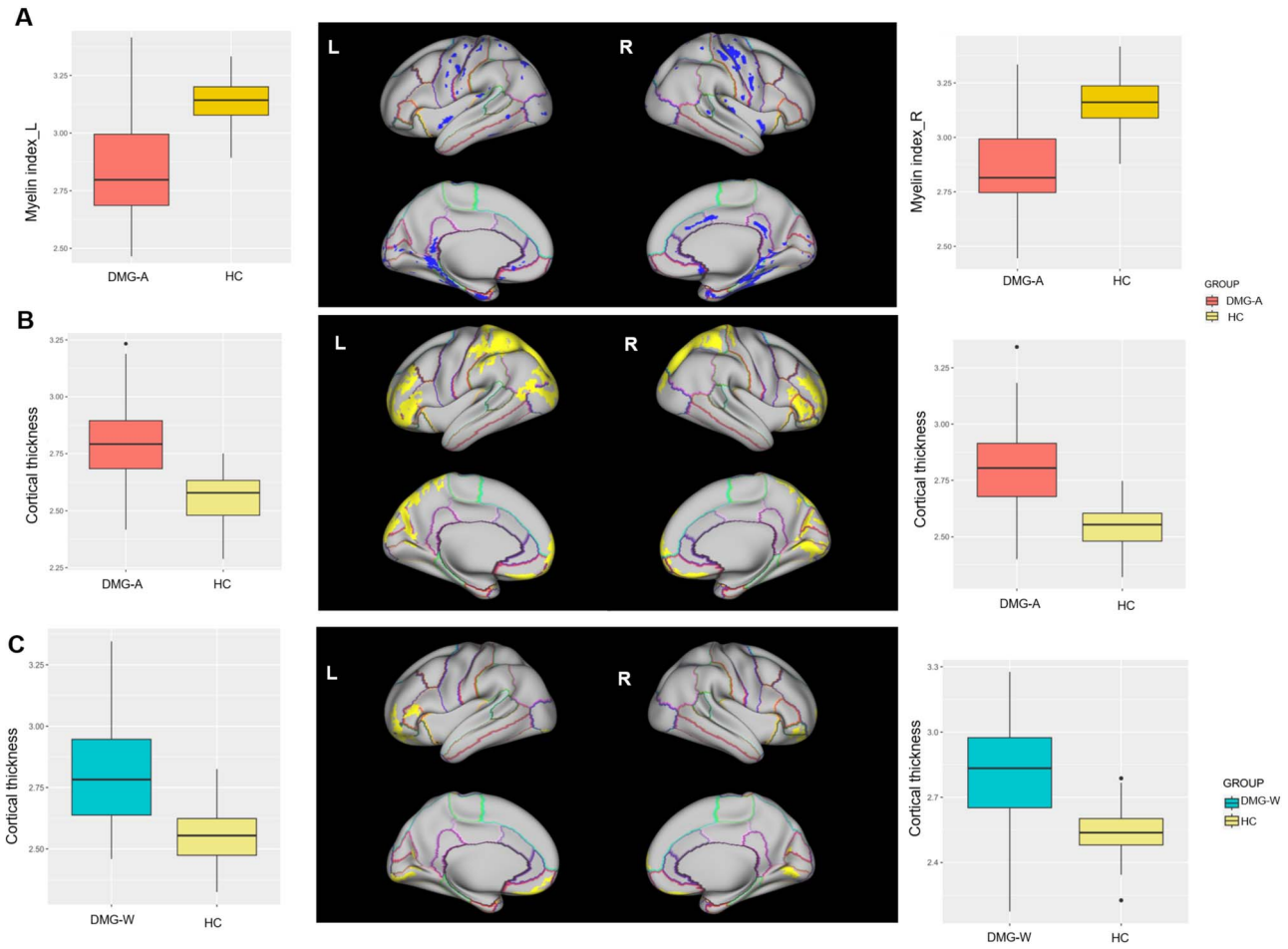

Fig. 2. Cortial myelin and thickness differences between patients' group and HC. The upper panel (A) exhibits reduced myelin content, while the lower panel (B) displays increased cortical thickness in the comparison between the DMG-A group and HC. The boxplots on both sides showed the distribution of myelin index and cortical thickness in significant clusters of left and right hemisphere, respectively. In panel (C), regions (in yellow) exhibiting increased thickness in the comparison between the DMG-W group and HC. Similarly, boxplots on both sides showed the distribution of thickness index in significant clusters of left and right hemisphere, respectively. Abbreviations: DMG-A, diffuse midline glioma with H3 K27-altered; DMG-W, diffuse midline glioma with H3 K27 wild-type; HC, healthy controls.

prediction model increased to 0.84 (Fig. 5B). Detailed model performance was shown in Table S1.

Discussion

It was the aim of our study to investigate whether DMG leads to whole-brain cortical structural alternations and whether there are distinct patterns of alteration between the DMG-A and DMG-W groups. For this purpose, we employed two potential metrics, namely cortical myelin (measured by T1w/T2w ratio) and cortical thickness, in our evaluation of DMG patients. Compared to HC, we found that both DMG-A and DMG-W induced widespread cortical thickness compensation in normal-appearing cortex. Regarding cortical myelin, DMG-A patients showed demyelination in regions of the sensorimotor network (SMN), default mode network (DMN), and salience network (SN), whereas DMG-W patients exhibited myelin content well preserved. Moreover, the observed demyelination in MOFG and increased cortical thickness in

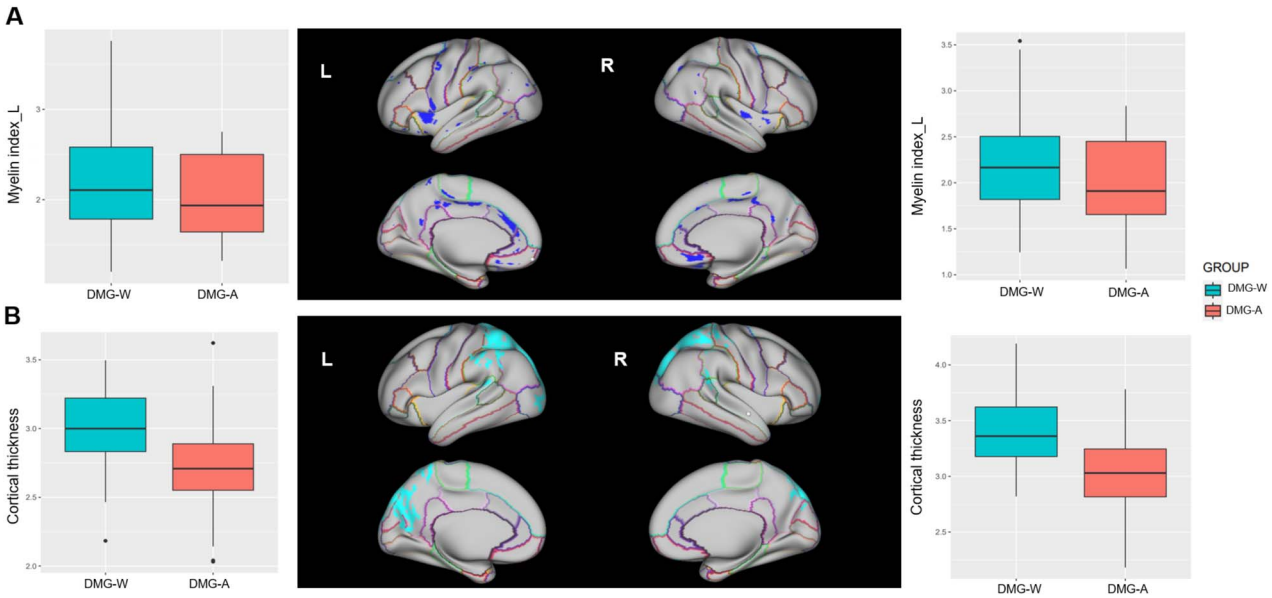

Fig. 3. Cortial myelin and thickness differences between DMG-A and DMG-W. The upper panel (A) represents regions with reduced myelin content, while the lower panel (B) represents regions with decreased cortical thickness. The boxplots on both sides showed the distribution of myelin index and cortical thickness in significant clusters of left and right hemisphere, respectively. Abbreviations: DMG-A, diffuse midline glioma with H3 K27-altered; DMG-W, diffuse midline glioma with H3 K27 wild-type; HC, healthy controls.

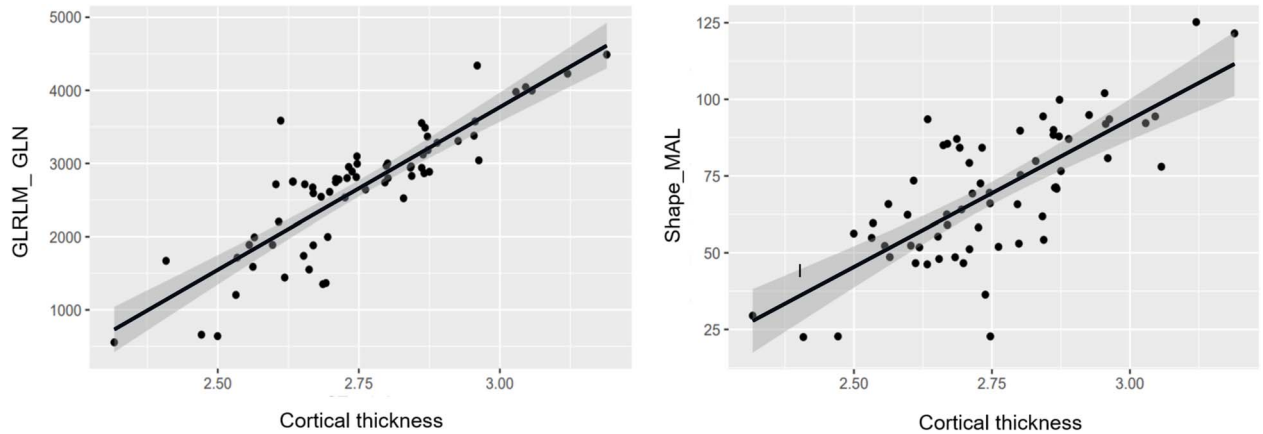

Fig. 4. Scatterplots showing positive correlations between average cortical thickness of the bilateral frontal, parietal, and occipital lobes in DMG-A group and radiomics features. Abbreviations: DMG-A, diffuse midline glioma with H3 K27-altered; GLRLM_GLN, gray level run length matrix of gray level non-uniformity; Dhape_MAL, shape of major axis length.

parietal and occipital regions may hold promise as potential biomarkers for distinguishing the DMG-A subtype. Finally, whole-brain cortical myelin and thickness demonstrated potential value in short-term survival prediction in DMG patients.

Cortical thickness compensations

Previous research has investigated remote morphometric alternations induced by glioma. Almairac et al. reported that insular glioma leads to greater gray matter volume in contralateral insular (Almairac et al. 2018). Similarly, another study revealed that frontal glioma triggered structural reorganization with increased cortical thickness in superior parietal cortex in the contralateral hemisphere (Liu et al. 2020). In the current study, when glioma invaded the midline tissues, we also observed significantly increased cortical thickness in widespread remote regions. Drawing from the principles of neuroplasticity, the human brain possesses the capacity to reorganize itself in response to glioma presence (Desmurget et al. 2007; Duffau 2014). Consequently, we speculate that the observed thickening of the cortex in the frontal, parietal, and occipital regions may serve a critical role in compensating for functional deficits arising from injury to midline structures. At a microscopic level, the precise cellular mechanisms underlying these changes remain unclear. However, potential contributors may include the formation of new synapses (Andoh and Koyama 2021) and the activation of microglial cells (Duffau 2005), both of which can be radiologically manifested as increased cortical thickness (Desmurget et al. 2007).

In the comparison between the DMG-A and DMG-W groups, we noted that the DMG-W group exhibited more prominent cortical thickening in bilateral parietal and occipital regions. It is well-established that H3 K27-altered status is linked to a more aggressive biological behavior and shorter overall survival when contrasted with H3 K27 wild-type (Ryall et al. 2016; Karremann et al. 2018). In simpler terms, DMG-W patients tend to display characteristics of slower tumor growth and less invasiveness, which may provide ample time for the cortical remodeling process

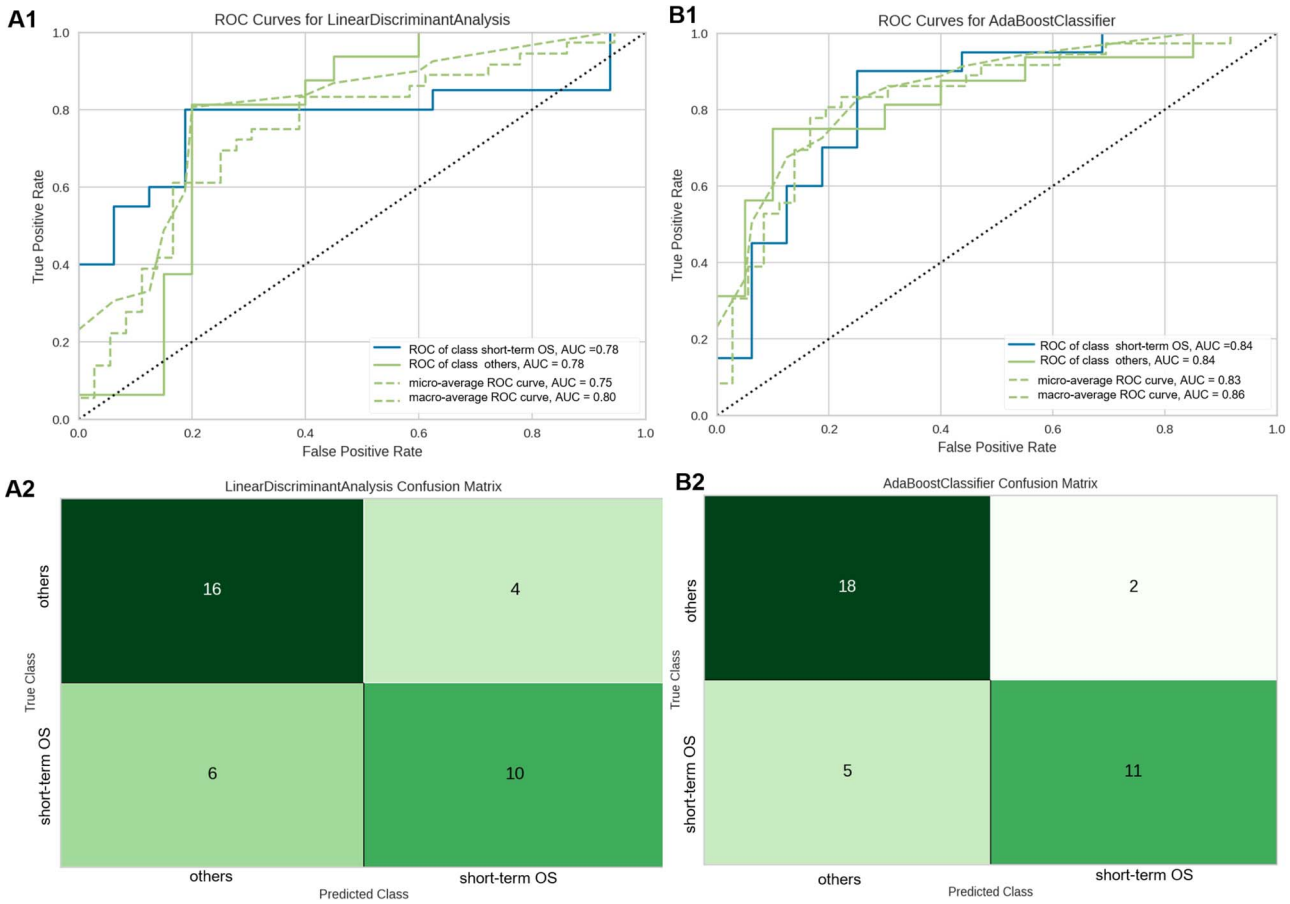

Fig. 5. Receiver operating characteristic curves and confusion matrices of the best-performing prediction models built on different feature set. (A1, A2) Utilizing the radiomics feature set radiomics feature set. (B1, B2) Integrating cortical metrics combined with radiomics.

to occur, potentially leading to more marked elevated cortical thickness.

Cortical demyelination

Previous work has extensively investigated microstructural changes of WM fiber integrity in patients with glioma. Latini et al. demonstrated a link between WM diffusion metrics and diffuse glioma early infiltration (Latini et al. 2021). Wang et al. found that insular glioma damaged the microstructure architecture of WM proximal to the tumor based on tract-based spatial statistics (Wang et al. 2022). Further, Zhang et al. revealed WM disruption was also occurred in contralateral hemisphere, indicating that chronic damage induce by frontal glioma may lead to remote fiber bundle degeneration (Zhang et al. 2023). Along with above perspectives, it is plausible to infer that such damage may also extend to the myelinated axons in the cortical mantle. Unlike the dense and consistently aligned myelinated axons in subcortical WM tracts, intracortical myelinated axons exhibit a less uniform and less dense arrangement, making traditional diffusion imaging difficult to measure. Glasser and van Essen first introduced a non-invasive technique for mapping in vivo intracortical myelin, which has since been widely used to investigate the effects of disease states on intracortical myelin (Glasser and Van Essen 2011), but it has never previously been used to assess whole-brain tumor burden in patients with DMG. In the current study, we identified that patients with DMG-A showed lower cortical myelin content in regions of the SMN (PreCG and PoCG), SN (insular, cACG, and PCG), and DMN (PHG, FG, and ICG).

It is not surprising that there is an abnormal myelin content associated with the SMN, as motor deficit is a common symptom in DMG-A. As the sites of primary sensory and motor cortex, the PreCG and PoCG have the functional characteristics of supporting the movement of the side limbs, and the characteristic of sensory projection is the left and right cross, respectively. Therefore, lower cortical myelin content in the bilateral PreCG and PoCG may indicate that the DMG-A cells have the ability to infiltrate the cortical myelinated axons, resulting in the damage of myelin in the sensorimotor cortex. As for SN, which plays a crucial role in selecting meaningful stimuli from an array of sensory input (Menon and Uddin 2010). At a regional level, patients with DMG-A showed demyelination in three of the four SN specific ROIs (insula, and ACG and PCG). The most significant change was seen in the insula, which has specifically been proposed as a "causal outflow hub" driving the switch between the DMN and central executive network, with anterior insula dysfunction and consequently impaired network switching implicated in other disorders demonstrating impaired executive control (Sridharan et al. 2008). Our findings of reduced myelin in SN nodes may explain some of the clinically documented cognitive challenges experienced by these patients (Yang et al. 2021). The DMN is a task-negative network, meaning it is the most prominent network activated during rest and internally driven processes such as mind wandering or future planning, previous studies have found disrupted connections in DMN in glioma patients based on diffusion tensor imaging (Jütten et al. 2021). This study further demonstrated the presence of altered cortical myelin within the DMN regions,

suggesting that DMN altered in DMG-A may be a part of the pathological changes associated with cognitive impairment.

Aside from above the regions, lower myelin content in MOFG were additionally observed when comparing DMG-A group with DMG-W group. The MOFG is involved in decision making and expectation. This finding fits well with the result found in Mattavelli et al., which indicated glioma patients performed worse on the gambling task (Mattavelli et al. 2012). Taken together with this previous study, we speculate that DMG-A patients may be more susceptible to impaired decision-making.

Notably, there was no significant brain cluster was found in cortical myelin content between the DMG-W group and HC. The DMG-W group is less invasive than the DMG-A group (Karremann et al. 2018). Lower aggressiveness implies lower cell-level protein and lower cell proliferation in the H3 K27 wild-type, even though they may induce the damage of the deep WM tracts; however, such damage may not extend to the myelinated axons in the cortical sheath, and thus reflecting the preserved myelin content.

Correlation between cortical morphology and DMG radiomics features

We found that higher GLRLM_GLN and Shape_MAL of DMG-A were correlated with increased cortical thickness in the clusters of in frontal, parietal, and occipital regions. GLN measures the similarity of gray-level intensity values in the image, where a higher GLN value indicated a lower similarity in intensity values (Cheung et al. 2023). GLN has been considered to be an important radiomics feature for determine glioma grade (Deng and Zhu 2023). Additionally, a prior study has demonstrated shape features are the most important radiomics feature for the prediction of H3 K27 mutation (Su et al. 2020). Our results further confirmed that radiomic features, especially GLRLM and shape, may have potential to serve as noninvasive biomarkers, capturing cortical morphology alternations in DMG-A patients. However, further verification is needed through future studies based on a larger sample size and multiple centers.

Classification potential of cortical metrices

In the current study, though the AUC of the best radiomics model in the testing cohort reaching 0.78 for short-term survival prediction, while after incorporating the cortical information into the radiomics model, the AUC of prediction model increased to 0.84. Considering that systemic infiltration is a hallmark of DMG pathogenesis, the integration of cortical metrics into the prediction model can provide a more comprehensive set of features, aiding in the comprehension of the pathological processes underlying DMG. From a translational perspective, our classification model demonstrates the potential to enhance prognosis determination and patient stratification through automated imaging analysis software within clinical settings. This entails the incorporation of various data processing and modeling procedures, which could assist clinical decision making in future.

This study has several limitations that should be acknowledged. Firstly, owing to the retrospective nature of our investigation, access to neurocognitive performance data for the patients was regrettably unavailable. Consequently, future longitudinal studies should consider incorporating these measures to investigate their potential associations with cortical structural alterations. Furthermore, the study is constrained by its relatively small sample size and the absence of an independent external validation dataset. To corroborate and expand upon our current findings, future research endeavors should encompass larger cohorts drawn from diverse institutions.

Conclusions

Utilizing comprehensive whole-brain cortical mapping, our study revealed that DMG has the capacity to induce cortical thickness compensation while concurrently leading to cortical demyelination in numerous non-lesional regions. These invisible alternations on conventional MRI and cortical features are correlated with patient short-term survival. The exploration of cortical thickness and myelin may provide a valuable tool for precise treatment for patients with DMG.

Author contributions

Simin Zhang (Conceptualization, Data curation, Investigation, Methodology, Project administration, Resources, Software, Validation, Writing—original draft), Xibiao Yang (Data curation, Visualization), Qiaoyue Tan (Data curation, Investigation, Resources), Huaiqiang Sun (Methodology, Software), Di Chen (Data curation, Formal analysis), Yinying Chen (Data curation), Hongjing Zhang (Data curation, Visualization), Yuan Yang (Funding acquisition, Investigation, Resources), Qiyong Gong (Conceptualization, Funding acquisition, Project administration, Supervision, Writing—review and editing), Qiang Yue (Conceptualization, Funding acquisition, Project administration, Supervision, Validation, Writing—review and editing).

Supplementary material

Supplementary material is available at *Cerebral Cortex* online.

Funding

This work was supported by the National Natural Science Foundation of China (Grant Nos 82271961, 81761128023, 81820108018, 81974278, 82027808), the National Key R&D Program of China (2022YFC2009900), NIH/NIMH R01MH112189-01, Sichuan Provincial Foundation of Science and Technology (Grant Nos 2019YFS0428, 2023YFG0127).

Conflict of interest statement: None declared.

Data sharing statement

The datasets produced during the course of this study can be obtained upon request directed to the corresponding author.

References

Almairac F, Duffau H, Herbet G. Contralesional macrostructural plasticity of the insular cortex in patients with glioma: a VBM study. *Neurology*. 2018:91(20):e1902–e1908.

Andoh M, Koyama R. Microglia regulate synaptic development and plasticity. *Dev Neurobiol*. 2021:81(5):568–590.

Cheung EYW, Wu RWK, Li ASM, Chu ESM. AI deployment on GBM diagnosis: a novel approach to analyze histopathological images using image feature-based analysis. *Cancer*. 2023:15(20):5063.

Chintagumpala M, Eckel SP, Krailo M, Morris M, Adesina A, Packer R, Lau C, Gajjar A. A pilot study using carboplatin, vincristine, and temozolomide in children with progressive/symptomatic low-grade glioma: a children's oncology group study†. *Neuro-Oncology*. 2015:17(8):1132–1138.

Deng S, Zhu Y. Prediction of glioma grade by tumor heterogeneity radiomic analysis based on multiparametric MRI. *Int J Comput Intell Syst*. 2023:16(1):51.

Desmurget M, Bonnetblanc F, Duffau H. Contrasting acute and slow-growing lesions: a new door to brain plasticity. *Brain*. 2007:130(Pt 4):898–914.

Duffau H. Lessons from brain mapping in surgery for low-grade glioma: insights into associations between tumour and brain plasticity. *Lancet Neurol*. 2005:4(8):476–486.

Duffau H. Diffuse low-grade gliomas and neuroplasticity. *Diagn Interv Imaging*. 2014:95(10):945–955.

Duffau H. White matter tracts and diffuse lower-grade gliomas: the pivotal role of myelin plasticity in the tumor pathogenesis, infiltration patterns, functional consequences and therapeutic management. *Front Oncol*. 2022:12:855587.

Fernandez-Alvarez M, Atienza M, Cantero JL. Effects of non-modifiable risk factors of Alzheimer's disease on intracortical myelin content. *Alzheimers Res Ther*. 2022:14(1):202.

Fischl B. FreeSurfer. *NeuroImage*. 2012:62(2):774–781.

Giese A, Westphal M. Glioma invasion in the central nervous system. *Neurosurgery*. 1996:39(2):235–252.

Glasser MF, Van Essen DC. Mapping human cortical areas in vivo based on myelin content as revealed by T1- and T2-weighted MRI. *J Neurosci*. 2011:31(32):11597–11616.

Glasser MF, Coalson TS, Robinson EC, Hacker CD, Harwell J, Yacoub E, Ugurbil K, Andersson J, Beckmann CF, Jenkinson M, et al. A multi-modal parcellation of human cerebral cortex. *Nature*. 2016:536(7615):171–178.

Hoffman LM, Veldhuijzen van Zanten SEM, Colditz N, Baugh J, Chaney B, Hoffmann M, Lane A, Fuller C, Miles L, Hawkins C, et al. Clinical, radiologic, pathologic, and molecular characteristics of long-term survivors of diffuse intrinsic pontine glioma (DIPG): a collaborative report from the International and European Society for Pediatric Oncology DIPG Registries. *J Clin Oncol*. 2018:36(19):1963–1972.

Isensee F, Jaeger PF, Kohl SAA, Petersen J, Maier-Hein KH. nnU-Net: a self-configuring method for deep learning-based biomedical image segmentation. *Nat Methods*. 2021:18(2):203–211.

Jütten K, Weninger L, Mainz V, Gauggel S, Binkofski F, Wiesmann M, Merhof D, Clusmann H, Na C-H. Dissociation of structural and functional connectomic coherence in glioma patients. *Sci Rep*. 2021:11(1):16790.

Karremann M, Gielen GH, Hoffmann M, Wiese M, Colditz N, Warmuth-Metz M, Bison B, Claviez A, van Vuurden DG, von Bueren AO, et al. Diffuse high-grade gliomas with H3 K27M mutations carry a dismal prognosis independent of tumor location. *Neuro-Oncology*. 2018:20(1):123–131.

Latini F, Fahlström M, Beháňová A, Sintorn IM, Hodik M, Staxäng K, Ryttlefors M. The link between gliomas infiltration and white matter architecture investigated with electron microscopy and diffusion tensor imaging. *Neuroimage Clin*. 2021:31:102735.

Liu Y, Hu G, Yu Y, Jiang Z, Yang K, Hu X, Li Z, Liu D, Zou Y, Liu H, et al. Structural and functional reorganization within cognitive control network associated with protection of executive function in patients with unilateral frontal gliomas. *Front Oncol*. 2020:10:794.

Louis DN, Perry A, Reifenberger G, von Deimling A, Figarella-Branger D, Cavenee WK, Ohgaki H, Wiestler OD, Kleihues P, Ellison DW. The 2016 world health organization classification of tumors of the central nervous system: a summary. *Acta Neuropathol*. 2016:131(6):803–820.

Louis DN, Perry A, Wesseling P, Brat DJ, Cree IA, Figarella-Branger D, Hawkins C, Ng HK, Pfister SM, Reifenberger G, et al. The 2021 who classification of tumors of the central nervous system: a summary. *Neuro-Oncology*. 2021:23(8):1231–1251.

Mattavelli G, Casarotti A, Forgiarini M, Riva M, Bello L, Papagno C. Decision-making abilities in patients with frontal low-grade glioma. *J Neuro-Oncol*. 2012:110(1):59–67.

Mendez Colmenares A, Voss MW, Fanning J, Salerno EA, Gothe NP, Thomas ML, McAuley E, Kramer AF, Burzynska AZ. White matter plasticity in healthy older adults: the effects of aerobic exercise. *NeuroImage*. 2021:239:118305.

Menon V, Uddin LQ. Saliency, switching, attention and control: a network model of insula function. *Brain Struct Funct*. 2010:214(5–6):655–667.

Nerland S, Jørgensen KN, Nordhøy W, Maximov II, Bugge RAB, Westlye LT, Andreassen OA, Geier OM, Agartz I. Multisite reproducibility and test-retest reliability of the T1w/T2w-ratio: a comparison of processing methods. *NeuroImage*. 2021:245:118709.

Nieuwenhuys R. The myeloarchitectonic studies on the human cerebral cortex of the Vogt-Vogt school, and their significance for the interpretation of functional neuroimaging data. *Brain Struct Funct*. 2013:218(2):303–352.

Nieuwenhuys R, Broere CA. A map of the human neocortex showing the estimated overall myelin content of the individual architectonic areas based on the studies of Adolf Hopf. *Brain Struct Funct*. 2017:222(1):465–480.

Noon A, Galban S. Therapeutic avenues for targeting treatment challenges of diffuse midline gliomas. *Neoplasia*. 2023:40:100899.

Osswald M, Jung E, Sahm F, Solecki G, Venkataramani V, Blaes J, Weil S, Horstmann H, Wiestler B, Syed M, et al. Brain tumour cells interconnect to a functional and resistant network. *Nature*. 2015:528(7580):93–98.

Price SJ, Allinson K, Liu H, Boonzaier NR, Yan J-L, Lupson VC, Larkin TJ. Less invasive phenotype found in isocitrate dehydrogenase–mutated glioblastomas than in isocitrate dehydrogenase wild-type glioblastomas: a diffusion-tensor imaging study. *Radiology*. 2016:283(1):215–221.

Righart R, Biberacher V, Jonkman LE, Klaver R, Schmidt P, Buck D, Berthele A, Kirschke JS, Zimmer C, Hemmer B, et al. Cortical pathology in multiple sclerosis detected by the T1/T2-weighted ratio from routine magnetic resonance imaging. *Ann Neurol*. 2017:82(4):519–529.

Rowley CD, Tabrizi SJ, Scahill RI, Leavitt BR, Roos RAC, Durr A, Bock NA. Altered intracortical T(1)-weighted/T(2)-weighted ratio signal in Huntington's disease. *Front Neurosci*. 2018:12:805.

Ryall S, Krishnatry R, Arnoldo A, Buczkowicz P, Mistry M, Siddaway R, Ling C, Pajovic S, Yu M, Rubin JB, et al. Targeted detection of genetic alterations reveal the prognostic impact of H3K27M and MAPK pathway aberrations in paediatric thalamic glioma. *Acta Neuropathol Commun*. 2016:4(1):93.

Sahm F, Capper D, Jeibmann A, Habel A, Paulus W, Troost D, von Deimling A. Addressing diffuse glioma as a systemic brain disease with single-cell analysis. *Arch Neurol*. 2012:69(4):523–526.

Sievers P, Sill M, Schrimpf D, Stichel D, Reuss DE, Sturm D, Hench J, Frank S, Krskova L, Vicha A, et al. A subset of pediatric-type thalamic gliomas share a distinct DNA methylation profile, H3K27ME3 loss and frequent alteration of EGFR. *Neuro-Oncology*. 2021:23(1):34–43.

Sridharan D, Levitin DJ, Menon V. A critical role for the right fronto-insular cortex in switching between central-executive and default-mode networks. *Proc Natl Acad Sci U S A*. 2008:105(34):12569–12574.

Su X, Chen N, Sun H, Liu Y, Yang X, Wang W, Zhang S, Tan Q, Su J, Gong Q, et al. Automated machine learning based on radiomics features predicts H3 K27M mutation in midline gliomas of the brain. *Neuro-Oncology*. 2020:22(3):393–401.

Thust S, Micallef C, Okuchi S, Brandner S, Kumar A, Mankad K, Wastling S, Mancini L, Jäger HR, Shankar A. Imaging characteristics of H3 K27M histone-mutant diffuse midline

glioma in teenagers and adults. *Quant Imaging Med Surg*. 2020:11(1):43–56.

Wang J, Xu S-L, Duan J-J, Yi L, Guo Y-F, Shi Y, Li L, Yang Z-Y, Liao X-M, Cai J, et al. Invasion of white matter tracts by glioma stem cells is regulated by a NOTCH1–SOX2 positive-feedback loop. *Nat Neurosci*. 2019:22(1):91–105.

Wang X, Zhou C, Wang Y, Wang L. Microstructural changes of white matter fiber tracts induced by insular glioma revealed by tract-based spatial statistics and automatic fiber quantification. *Sci Rep*. 2022:12(1):2685.

Winkler AM, Ridgway GR, Webster MA, Smith SM, Nichols TE. Permutation inference for the general linear model. *NeuroImage*. 2014:92(100):381–397.

Yang J, Gohel S, Zhang Z, Hatzoglou V, Holodny AI, Vachha BA. Glioma-induced disruption of resting-state functional connectivity and amplitude of low-frequency fluctuations in the salience network. *AJNR Am J Neuroradiol*. 2021:42(3):551–558.

Zhang P, Gu G, Duan Y, Zhuo Z, Pan C, Zuo P, Wang Y, Li X, Jiang Z, Qu L, et al. White matter alterations in pediatric brainstem glioma: an national brain tumor registry of China study. *Front Neurosci*. 2022:16:986873.

Zhang S, Zhao F, Yang X, Tan Q, Li S, Shao H, Su X, Gong Q, Yue Q. Multiparametric mapping of white matter reorganizations in patients with frontal glioma-related epilepsy. *CNS Neurosci Ther*. 2023:29(8):2366–2376.